WELDING RESEARCH

SUPPLEMENT TO THE *WELDING JOURNAL,* JUNE 2003
Sponsored by the American Welding Society and the Welding Research Council

Microstructural Evolution and Weldability of Dissimilar Welds between a Super Austenitic Stainless Steel and Nickel-Based Alloys

The influence of filler metal composition and dilution on fusion zone microstructure and solidification cracking susceptibility is evaluated for AL-6XN welded to IN622 and IN625

BY J. N. DUPONT, S. W. BANOVIC, AND A. R. MARDER

ABSTRACT. Microstructural evolution and solidification cracking susceptibility of dissimilar metal welds between AL-6XN super austenitic stainless steel and two nickel-based alloys, IN625 and IN622, were studied using a combination of electron microscopy, differential thermal analysis, and Varestraint testing techniques. Welds were prepared over the entire dilution range (where dilution was determined with respect to AL-6XN as the base metal). The effect of processing parameters and filler metal chemistry on the fusion zone composition, microstructure, and resultant weldability was investigated.

Iron additions to the weld (which occur with increasing dilution) increased the segregation potential of Mo and Nb. This behavior was attributed to a reduction in the solubility of Mo and Nb in austenite with increasing iron additions, as inferred from available binary phase diagrams. Welds prepared with IN622 formed a single interdendritic σ phase at the end of solidification, and the amount of this secondary phase was not sensitive to changes in dilution. The σ phase formed at a relatively high temperature and led to a relatively narrow solidification temperature range for welds prepared with IN622. In contrast, welds prepared with IN625 exhibited NbC and Laves phases in the interdendritic regions, and the total amount of secondary phase decreased with increasing dilution. Solidification of welds prepared with IN625 terminated with formation of the Laves constituent at relatively low temperature and, thus, the solidification temperature range of welds involving IN625 was relatively wide.

The solidification cracking sensitivity of welds prepared with IN622 was relatively low and independent of weld metal dilution level, while the cracking susceptibility of welds produced with IN625 was relatively high and increased with decreasing dilution. The dilution/cracking relation is controlled by the solidification temperature range and amount of secondary phase that forms at the terminal stages of solidification. The good cracking resistance of welds prepared with IN622 is attributed to the small amount of secondary phase and narrow solidification temperature range. The relatively poor cracking resistance of welds prepared with IN625 is attributed to a wide solidification temperature range and increasing amount of secondary phase that forms with decreasing dilution.

J. N. DUPONT is Associate Professor and Director, Joining and Laser Processing Laboratory, Department of Materials Science and Engineering, Lehigh University, Bethlehem, Pa. S. W. BANOVIC is Research Scientist, National Institute of Standards and Technology, Bethesda, Md. A. R. MARDER is Professor, Department of Materials Science and Engineering, Lehigh University, Bethlehem, Pa.

KEY WORDS

Solidification Cracking
Dissimilar Metals
Nickel-Based Alloys
Stainless Steel
Super Austenite
Cracking
GTAW
Gas Tungsten Arc

Introduction

Super austenitic stainless steels such as AL-6XN are used extensively in applications requiring good resistance to aqueous corrosion. These relatively high-nickel stainless steels contain Mo additions (~ 6–7 wt-%) for improved corrosion resistance. However, during solidification of the weld, Mo segregates preferentially to the liquid due to the low solubility of Mo in the austenite phase and leaves the first solid to form depleted in Mo (Ref. 1). In addition, the low diffusion rate of Mo in γ does not allow for Mo to diffuse back toward the dendrite cores to eliminate the concentration gradient. This can lead to poor corrosion resistance of the weld metal. Previous research has shown that the depleted dendrite cores are susceptible to preferential corrosion due to the low, localized Mo concentrations (Refs. 2–5). To compensate for this effect, high-Mo, nickel-based filler metals such as IN625 (~ 9 wt-% Mo) and IN622 (~ 14 wt-% Mo) are often utilized during fusion welding of these alloys (Ref. 5). While these filler metals do not eliminate microsegregation of Mo, the dendrite core compositions in the fusion zone are increased relative to those in autogeneous welds, and this helps to minimize preferential attack at the dendrite cores.

With this approach, the final distribution of Mo (and other alloying elements)

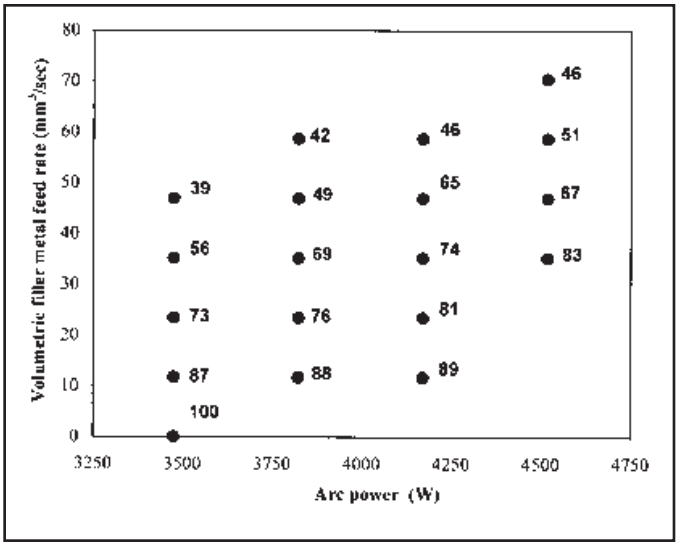

Fig. 1 — Experimental matrix of fusion welds produced where AL-6XN was the substrate and IN625 was the filler metal. Numbers to the right signify the dilution level with respect to AL-6XN as the substrate.

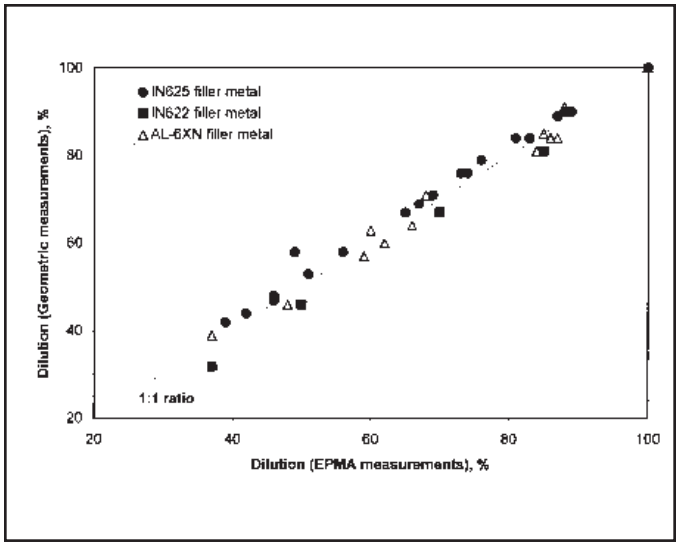

Fig. 2 — Comparison plot of dilution levels as determined through both geometric measurements and chemical analysis showing good agreement between the two methods.

Table 1 — Compositions for Raw Materials (wt-%)

	Filler Metal Diameter	Fe	Ni	Cr	Mo	Nb	Mn	Si	C
AL-6XN									
Filler metal	0.064	47.6	23.9	21.3	6.1	0.0	0.2	0.3	0.023
Plate		47.0	24.4	20.9	6.3	0.0	0.2	0.3	0.029
IN625									
Filler metal	0.035	0.6	64.6	21.7	8.9	3.5	0.0	0.1	0.010
Plate		4.5	60.8	20.8	8.7	3.5	0.1	0.2	0.080
IN622									
Filler metal	0.035	2.4	59.0	20.5	14.3	0.0	0.2	0.0	0.003
C-22									
Plate		3.6	56.7	21.3	13.2	0.0	0.2	0.0	0.013

will be controlled by the filler metal composition, welding parameters (which control the dilution and resultant nominal weld metal composition), and the segregation potential of each element. In addition, interactive effects may exist in which the segregation potential of an alloying element depends on the nominal weld composition. These factors, in turn, will govern the solidification behavior and resultant hot cracking susceptibility of the fusion zone. Therefore, since potentially wide ranges of weld metal composition are possible in practice, a large variation in fusion zone cracking susceptibility may be encountered. However, no detailed study has been reported that investigates the relationship between welding parameters, nominal weld composition, fusion zone microstructure, and resultant weldability. Thus, the objective of this research was to characterize the microstructures and weldability of fusion welds in AL-6XN stainless steel as a function of filler metal composition (using IN625 and IN622) and welding parameters. The results of this study will be useful for ultimately minimizing solidification cracking in welds of this alloy.

Experimental Procedure

Welds were produced between AL-6XN stainless steel and nickel-based alloys IN622 and IN625 over the entire dilution range using the gas tungsten arc welding (GTAW) process. With the GTAW process, the volumetric filler metal feed rate and arc power can be independently controlled, thus easily changing the dilution levels. The starting substrate materials were approximately 0.64 cm thick, 2.54 cm wide, and 15.25 cm in length. The samples were held flush to the welding table in order to maintain a constant and reproducible heat sink, with the table being at room temperature before beginning each deposit. The travel speed was fixed at 2.0 mm/s with a 2.5-mm arc length, which produced a voltage of 14 ± 1.3 V. Commercially pure argon was used as the shielding gas.

The materials used were AL-6XN and IN625 both in plate and filler metal form. A small heat of IN622 filler metal was obtained while C-22 (compositional equivalent for IN622) was used in plate form. Table 1 shows the respective compositions of all the materials. In order to produce dilution levels from 0 to 100%, with respect to AL-6XN as the base metal, IN625 and IN622 filler metal were deposited on AL-6XN for high dilution levels, typically above 50% dilution. For the lower values, the materials were reversed with AL-6XN filler metal being deposited onto IN625 and C-22 base metals.

Samples were removed from the welds, mounted in cold setting epoxy, and polished to a 0.04-μm finish using colloidal silica. Higher dilution level samples were electrolytically etched in a mixture of nitric acid (HNO_3) and water (H_2O) in the proportions of 60/40 using a platinum cathode at a preset voltage of 5 V. For the lower dilution levels, 10% oxalic acid was used under the same conditions. Microstructural characterization was performed using electron microscopy techniques. Dilution levels were determined by two methods: chemical analysis and geometric dilution calculations. For the former, quantitative chemical information was obtained through use of an electron probe microanalyzer (EPMA). A JEOL 733 SuperProbe EPMA, equipped with wavelength dispersive spectrometers, was operated at an accelerating voltage and probe current of 15 kV and 20 nA, respectively. Sampled areas were approximately 1500 μm^2, large enough to avoid

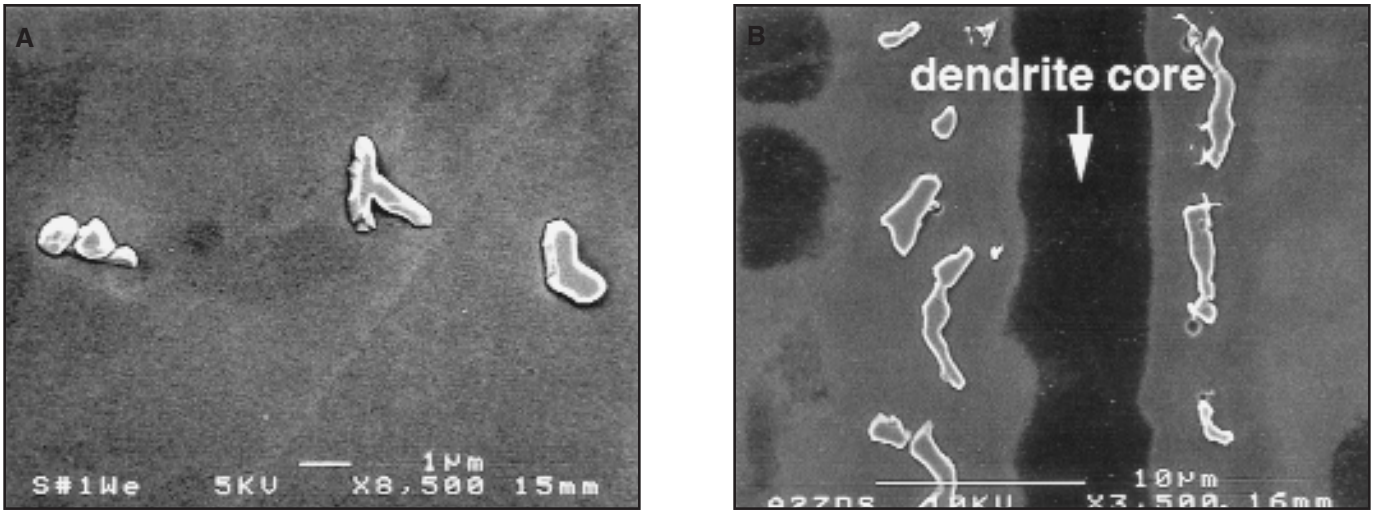

Fig. 3 — SEM photomicrographs of the typical phases observed in welds of AL-6XN (A) and welds prepared with the IN622 (B).

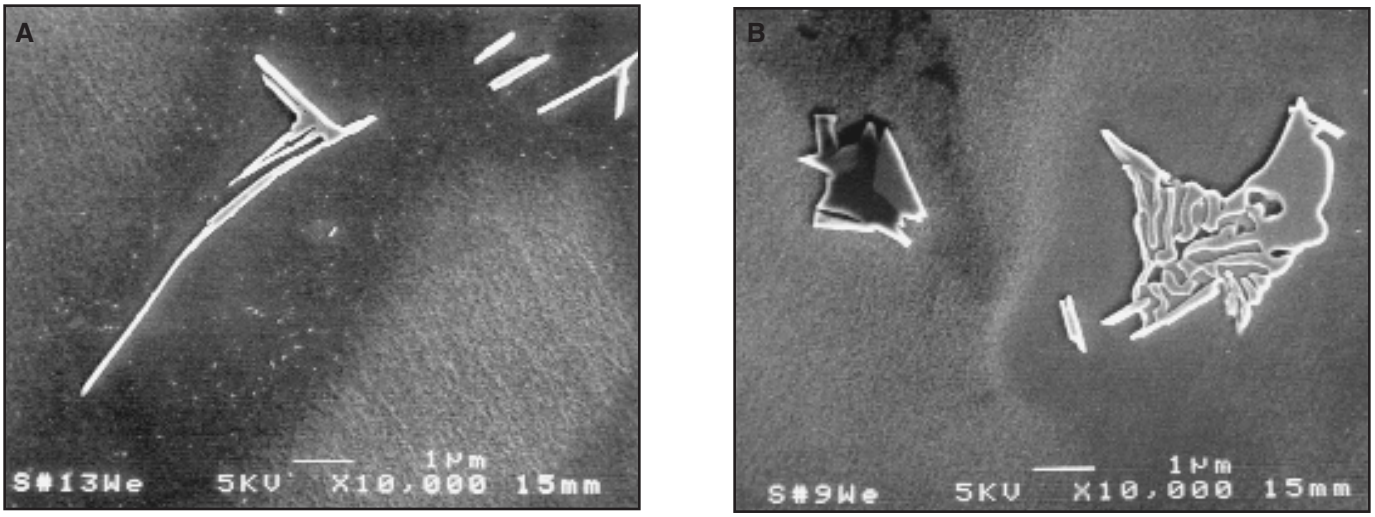

Fig. 4 — SEM photomicrographs of the typical phases observed in welds prepared with the IN625. A — "Chinese script;" B — eutectic-type.

any deviations that may be encountered due to microsegregation. X-ray counts were converted to weight percentages using a ZAF correction scheme (Ref. 6). EPMA traces were also conducted in spot mode (i.e., with no beam raster) in order to investigate microsegregation patterns from solidification.

In the fully mixed fusion zone, the final weld composition will simply be a mixture of the substrate and filler metal and is given by

$$C_{fz} = C_{fm}(1–D) + C_s(D) \quad (1)$$

where C_{fz}, C_{fm}, and C_s are the elemental compositions of the fusion zone, filler metal, and substrate, respectively, and D is the dilution level. Thus, when C_{fz}, C_{fm}, and C_s are all known, the dilution level is simply determined by

$$D = \frac{C_{fz} - C_{fm}}{C_s - C_{fm}} \quad (2)$$

The values for the major constituents of Fe and Ni were used and averaged to get the final dilution level of the weld. Dilution levels were also determined using metallographic methods to measure the individual geometric cross-sectional areas of the deposited filler metal and melted substrate. The ratio of the melted substrate (A_s) to the total melted cross-sectional area from the filler metal and substrate ($A_s + A_{fm}$) is the dilution level

$$D = \frac{A_s}{A_s + A_{fm}} \quad (3)$$

Solidification cracking susceptibility was determined using Varestraint testing with subsize specimens (165 x 25 x 3.2 mm). The crown of each weld deposit was first machined flush with the top surface of the plate. The back side of the surface was then machined to obtain the final 3.2-mm thickness. This process for making Varestraint samples from dissimilar welds was described previously in more detail (Ref. 1). A welding current of 100 A and 12 V was chosen for Varestraint testing so that the material melted during the autogeneous Varestraint pass resided entirely within the homogeneous portion of the original dissimilar metal weld fusion zone. (In this work, the "homogeneous portion" of the fusion zone refers to the fully mixed fusion zone where, on a macroscopic scale, the composition is uniform. In other words, the partially melted and partially mixed zones were avoided.) The travel

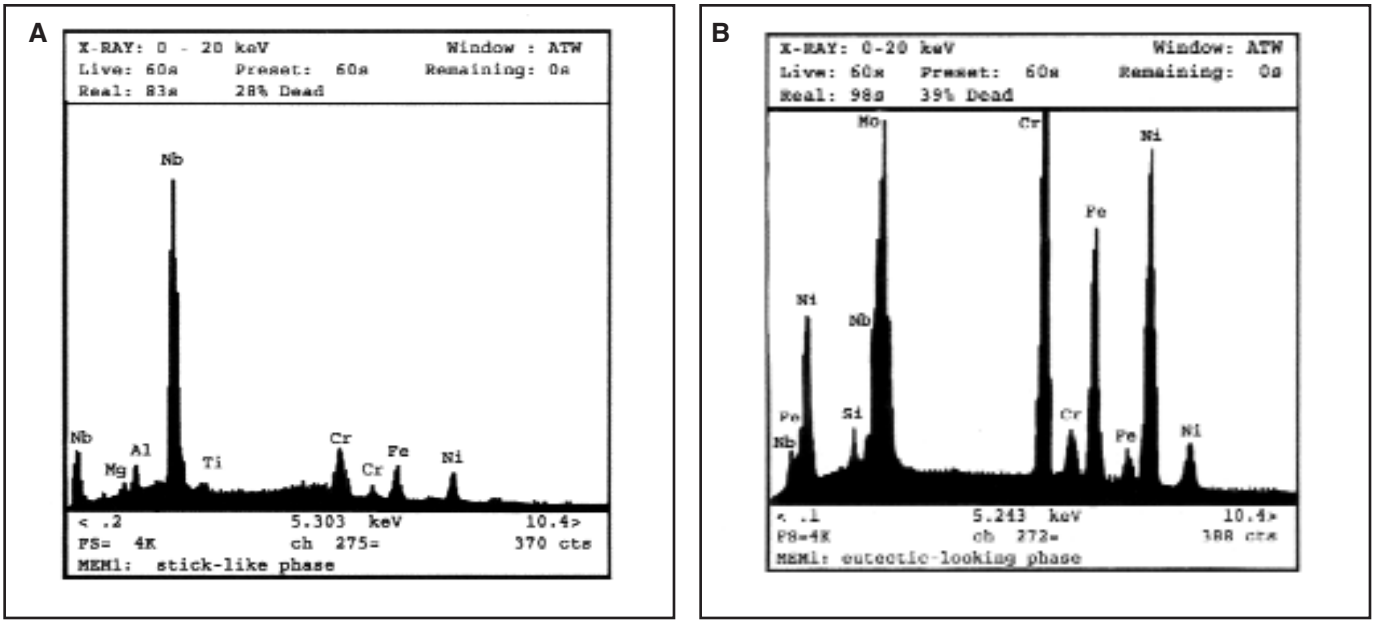

Fig. 5 — EDS spectra collected from NbC (A) and Laves (B) phases in weld prepared with IN625.

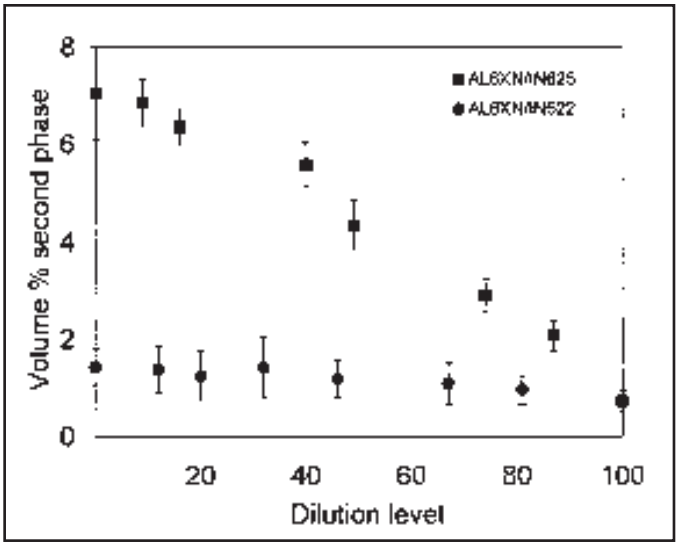

Fig. 6 — Amount of second phase measured in the fusion zone for both sets of dissimilar metal welds plotted as a function of dilution level.

speed was 3.3 mm/s while a high-purity argon gas was used for the shielding gas.

Three samples of each dilution level were tested at an augmented strain of 3.75%, which was determined to be the saturation strain from preliminary experiments. The standard deviation for 95% confidence interval for each crack length value was determined from the individual measurements. The crack lengths were measured perpendicular to the edge of the weld pool using a light optical microscope interfaced with the LECO 3001 quantitative image analysis system. The maximum crack length was defined as the longest crack for each sample, while the total crack length was the addition of all the crack lengths per sample.

Differential thermal analysis (DTA) was conducted on selected samples carefully sectioned out of the homogenous portion of the fusion zone of the dissimilar metal welds. Samples were heated to 10°C above their liquidus temperatures at 5°C/min and cooled at 20°C/min to room temperature. This procedure was conducted under flowing argon to avoid oxidation of the sample. The amount of second phase in each weld was measured by Quantitative Image Analysis on at least 20 fields for each dilution level, and the standard deviation for the 95% confidence interval was determined from the measurements.

Results and Discussion

Information on fusion zone compositions, microsegregation, and secondary phase formation are presented below. Detailed descriptions of these results have been provided in Refs. 7 and 8. The information is briefly summarized here, as it forms a basis for interpreting the weldability results, which are the main focus of this article.

Fusion Zone Compositions

The relation between dilution and welding parameters for these dissimilar welds has already been described in quantitative detail through process modeling in Ref. 7. The results will only be briefly summarized here to support the remaining sections on microstructural evolution and weldability. Welds were produced to obtain the full range of dilution levels for both sets of dissimilar metal welds between AL-6XN and IN625 or IN622. Volumetric filler metal feed rates between 0 and ~80 mm^3/s were used while the current was varied between 250 and 325 A in 25-A increments and voltages averaged 14 V ± 1.3 V. This produced a range of arc power (VI) from 3475 to 4520 W. Figure 1 displays a typical experimental matrix produced for samples where AL-6XN was the substrate and IN625 was the filler metal. Each data point represents a weld deposited at the specified volumetric filler metal feed rate and arc power. The numbers located to the right of the symbols signify the resultant dilution levels determined by EPMA measurements. Attempts were made to decrease the dilution to lower levels using AL-6XN as the substrate. However, a point was reached where the filler metal was not being completely melted and exited the weld pool still in solid form. Therefore, the full range of dilution and resultant weld metal com-

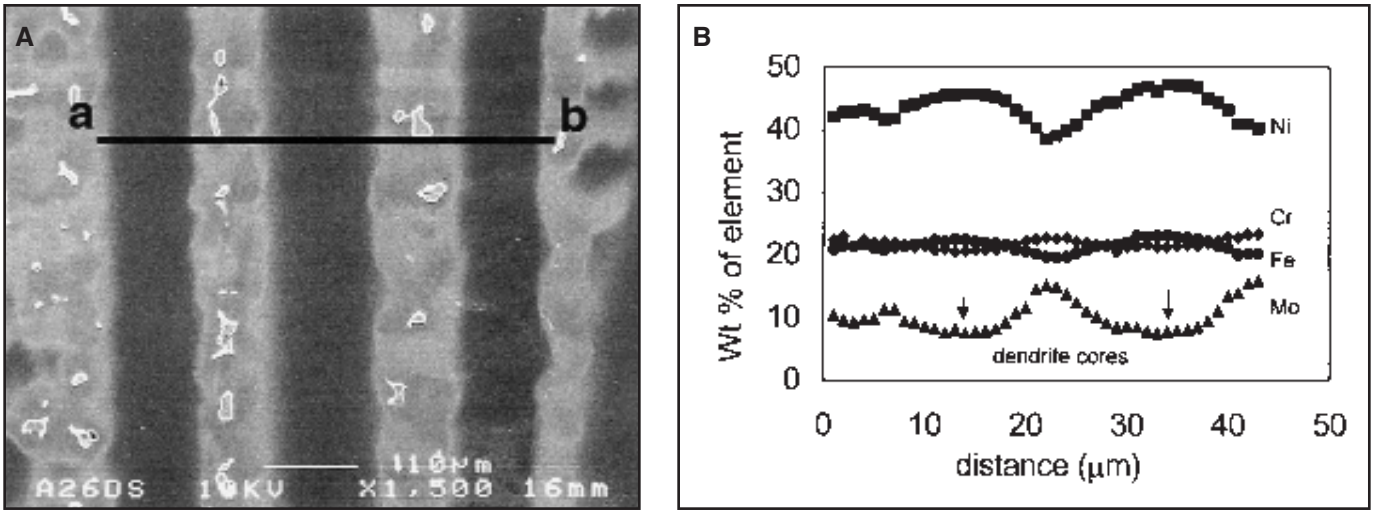

Fig. 7 — Characteristic segregation pattern found for dendritic structures of a dissimilar metal weld with IN622 filler metal, 32% dilution level. A — Analyzed area; B — microprobe trace.

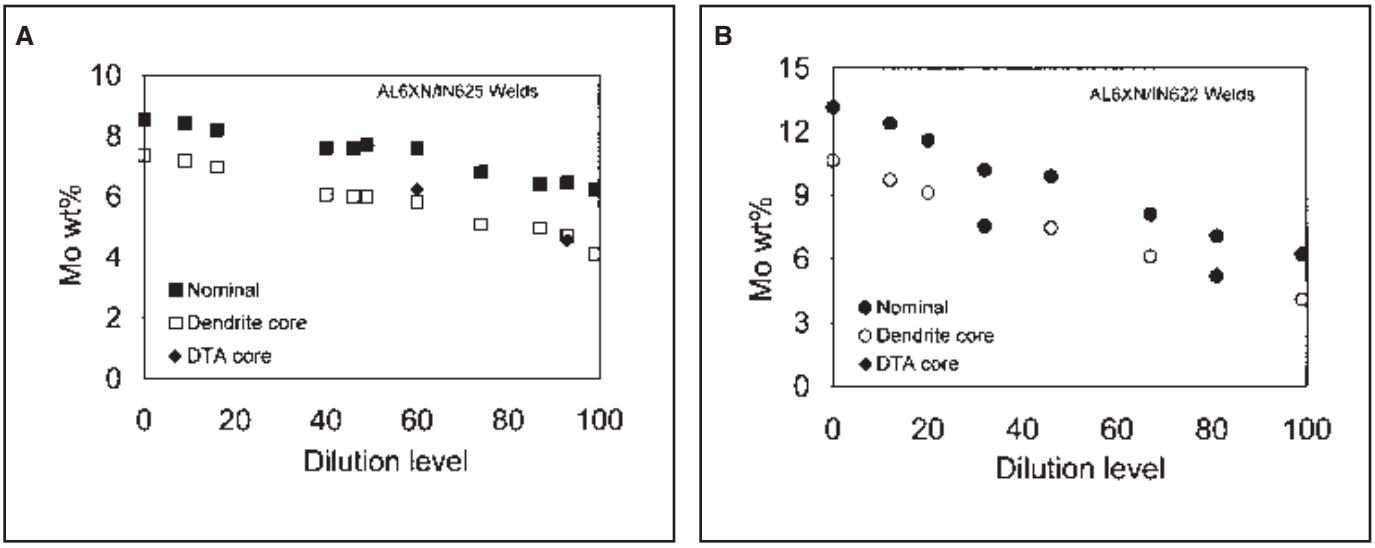

Fig. 8 — Nominal and dendrite core Mo compositions for the as-welded structures and DTA samples plotted as a function of dilution level. A — Welds prepared with IN625; B — welds prepared with IN622.

position was obtained by reversing the materials during the process and depositing AL-6XN filler metal onto the nickel-based substrates. Relatively good agreement can be seen over the entire range of samples between the two methods used to calculate the dilution levels, as shown in Fig. 2. More detail on these results can be found in Ref. 7.

Secondary Phase Formation and Microsegregation

Figure 3 shows SEM photomicrographs of the typical phases observed in autogeneous welds of AL-6XN (Fig. 3A) and welds prepared with IN622 — Fig. 3B. In these welds, an interdendritic phase was observed with a globular morphology. DTA samples from welds prepared with IN622 showed identical results. The interdendritic phase in the DTA samples was larger because of the slower cooling rates and could be analyzed by EPMA. Typical results are shown in Table 2. The composition of this phase is consistent with the sigma (σ) phase commonly observed in welds of both AL-6XN (Ref. 9) and IN622 (Ref. 10). As this phase is commonly found in welds of both AL-6XN and IN622, it is not surprising to find it in this set of dissimilar welds. Note that the sigma phase is very high in Cr and Mo.

Figure 4 shows SEM photomicrographs of the typical phase morphologies observed in welds prepared with IN625. There were two types of phases observed in these welds: one often referred to in the literature as a "Chinese script" morphology (Fig. 4A), and one with a eutectic-type morphology (Fig. 4B) (Refs. 11–14). Typical EDS spectra collected from the phase with the "Chinese script" and eutectic-type morphology are shown in Figs. 5A and 5B,

Table 2 — Composition of Second Phase[a]

Fe	Ni	Cr	Mo	Nb	Mn	Si
31.1	14.9	25.5	25.9	0.0	0.3	0.4
1.5	0.3	1.1	2.4	0.0	0.0	0.0

(a) Found within the interdendritic region of dissimilar metal weld samples prepared with IN622 after DTA testing. Compositions determined by EPMA, with all values reported in weight-percent. Values under reported compositions represent standard deviations.

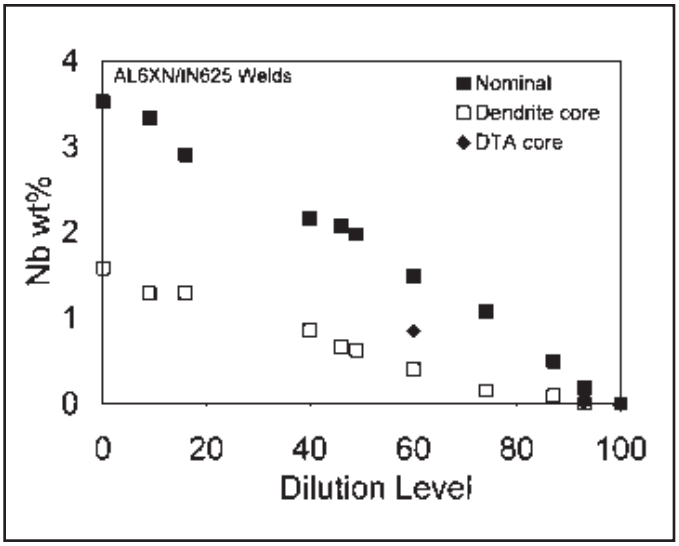

Fig. 9 — Nominal and dendrite core Nb compositions for the as-welded structures and DTA samples plotted as a function of dilution level for welds with IN625.

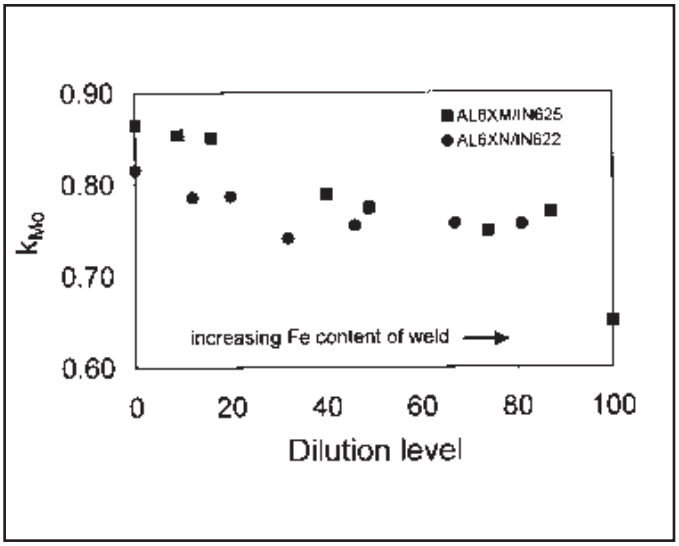

Fig. 10 — Mo partition coefficient as a function of dilution level for both sets of welds.

Table 3 — Partition Coefficient Values for Dissimilar Metal Welds with IN622

Dilution Level	100%	81%	67%	46%	32%	20%	12%	0%
Fe	1.06	1.09	1.07	1.17	1.16	1.09	1.04	1.06
Ni	1.02	1.06	1.09	1.03	1.02	1.07	1.07	1.04
Cr	0.99	0.91	0.92	0.91	0.94	0.89	0.93	0.95
Mo	0.65	0.76	0.76	0.75	0.74	0.79	0.79	0.82
Mn	0.76	0.74	0.87	0.87	0.80	0.86	0.84	0.82

Table 4 — Partition Coefficient Values for Dissimilar Metal Welds with IN625

Dilution Level	87%	74%	49%	46%	40%	16%	9%	0%
Fe	1.08	1.10	1.08	1.09	1.10	1.09	1.15	1.05
Ni	1.03	1.04	1.07	1.07	1.06	1.05	1.05	1.03
Cr	0.91	0.90	0.84	0.90	0.91	0.90	0.93	0.95
Mo	0.77	0.75	0.77	0.79	0.79	0.85	0.85	0.86
Nb	0.20	0.15	0.32	0.32	0.40	0.45	0.39	0.45
Mn	0.89	0.84	0.83	0.87	0.85	0.77	0.83	0.81

respectively. Note the "Chinese script" phase is very high in Nb. It has been well established that Nb-bearing superalloys terminate solidification by the formation of a NbC phase with this Chinese script morphology and a γ/Laves constituent that exhibits a eutectic-type morphology (Refs. 11–14). This is consistent with the SEM photomicrographs and EDS spectra shown in Figs. 4 and 5. Quantitative image analysis was used to measure the total amount of secondary phases that formed in each weld, and the results are shown in Fig. 6. The volume percent of secondary phase formed in welds prepared with IN625 decreased with increasing dilution levels. In contrast, the amount of secondary phase that formed in welds prepared with the IN622 filler metal was essentially insensitive to changes in dilution.

EPMA traces were conducted across the dendritic substructures found within the fusion zone of the welds and across the large cells of the DTA microstructures to investigate the segregation patterns that occurred upon solidification. Figure 7 shows a typical EPMA trace and the corresponding area that was analyzed. In all cases, the dendrite cores were depleted in Mo and Nb (the latter for alloys with IN625 only) and enriched in Fe and Ni. In general, Cr had a slight tendency to segregate to the liquid. Similar results were obtained for traces across the structures observed within the DTA samples.

EPMA traces were also conducted across the dendritic substructures in the unmixed zone of the dissimilar metal welds. In these areas of the fusion zone, the presence of the dendritic substructure was a direct indication that melting occurred, but EPMA traces showed the nominal Mo content was identical to the base metal, and thus no mixing with the filler metal occurred. On welds prepared with the AL-6XN base metal, EPMA scans showed the Mo concentration in the dendrite core in the unmixed zone was identical to the Mo dendrite core concentration in the fusion zone of an autogenous weld on AL-6XN. This is an important observation that indicates, regardless of the filler metal composition, an unmixed zone will always exist that contains dendrite core concentrations equivalent to that of an autogeneous weld. Thus, it is not possible to increase the core composition of the dendrites in the unmixed zone. The formation of unmixed zones in AL-6XN has been investigated previously (Ref. 5) and will not be described here further.

The amount of Mo and Nb in the dendrite cores for all the welds and DTA samples, as well as those for the nominal composition of the fusion zone, is plotted as a function of dilution level in Figs. 8 and 9. For both sets of data, as the dilution level increased, the amount of Mo and Nb were found to decrease in both the nominal and dendrite core compositions. It is interesting to note that, although the DTA samples were solidified at a rate of only

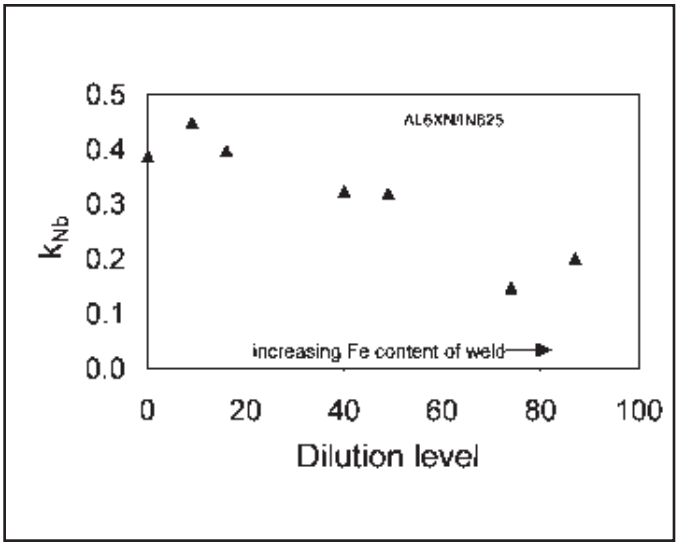

Fig. 11 — Nb partition coefficient as a function of dilution level for welds prepared with IN625.

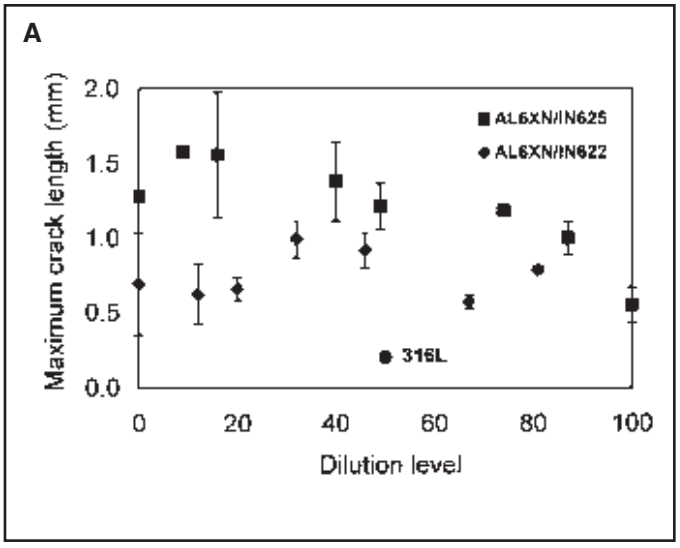

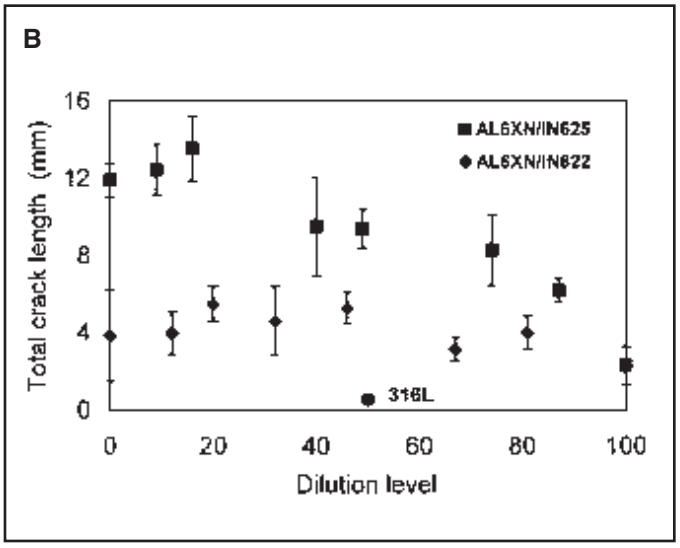

Fig. 12. Plots. A — Maximum crack length; B — total crack length as a function of the dilution.

20°C/min, the Mo core compositions are similar to those in the welds of identical nominal compositions. Thus, Mo segregation persists even under the slower cooling rate conditions used for DTA. The reasons for this have been explained in detail in Ref. 8. The dendrite Nb concentration (for welds prepared with IN625) is slightly higher in the DTA samples than those in the as-welded condition, indicating that some back diffusion of Nb can occur during the slow cooling rate used for DTA.

It is well known that solid-state diffusion of substitutional alloying elements (particularly Mo and Nb) in face-centered cubic alloys are insignificant under cooling rates typical of arc welding (Refs. 12, 14). Under this condition, the EPMA data can be used to determine the distribution coefficient (k) of each alloying element at the onset of solidification by $k = C_{core}/C_o$, where C_{core} is the core concentration and C_o is the nominal concentration of the element of interest. Tables 3 and 4 summarize the k-values of the major alloying elements for the welds investigated. These values are important from a corrosion perspective because they dictate the dendrite core composition of the weld. A k-value near unity indicates that particular element will show little tendency to segregate and the core composition will be close to the nominal composition. The lower the k value, the lower the dendrite core composition.

It can be seen that all of the matrix elements (Fe, Ni, Cr) show little tendency for segregation during solidification (k-values close to one). Since their values are larger than unity, Fe and Ni segregate to the solid, while Cr partitions to the liquid. The k-values for Mo are relatively low and span the range from 0.65 to 0.86. These values are in good agreement with other reported k_{Mo} values in similar alloy systems (Refs. 12, 13). As shown in Fig. 10, the Mo partition coefficient decreases as the iron content in the weld increases (i.e., as the dilution level increases). A similar trend is observed for Nb, as shown in Fig. 11. These effects are controlled by the influence of Fe on the solubility of Mo and Nb in austenite and can be explained by consulting the phase diagrams for the Ni-Mo, Fe-Mo, Ni-Nb, and Fe-Nb systems (Ref. 15). These diagrams indicate that the maximum solid solubility of Mo in γ-Ni is 35 wt-% (at 1200°C), while a maximum of only 2.9 wt-% Mo can be dissolved in γ-Fe (at ~1150°C). A similar trend is observed with Nb, where the maximum solid solubility of Nb in γ-Ni is 18.2 wt-% (at 1286°C), while it is only 1.3 wt-% at a similar temperature (1210°C) in γ-Fe. Based upon these observations, Fe additions to nickel-based alloys will decrease the solubility of Mo and Nb in austenite. Thus, as the Fe-rich dendrites form, the decreased solubility will lower the amount of Mo and Nb dissolved in the first solid, and increased segregation to the liquid will occur. The general trend of decreasing k-values for Mo and Nb with increasing Fe (Figs. 10 and 11) confirms this. Therefore, the segregation potential of Mo and Nb is a function of the nominal composition of the weld metal. Since the fusion zone composition depends on the arc power and volumetric filler metal feed speed, the segregation potential of Mo and Nb will be indirectly affected by the welding parameters.

The information presented above can be used to understand the microstructural evolution of welds prepared with each filler metal. In the case of welds made on "pure" AL-6XN and welds prepared with IN622 (each of which contain no Nb), Mo segregated from the solid to the liquid and the Mo-rich sigma (σ) phase formed at the terminal stages of solidification. Thus, solidification initiates by a $L \rightarrow \gamma$ (austenite)

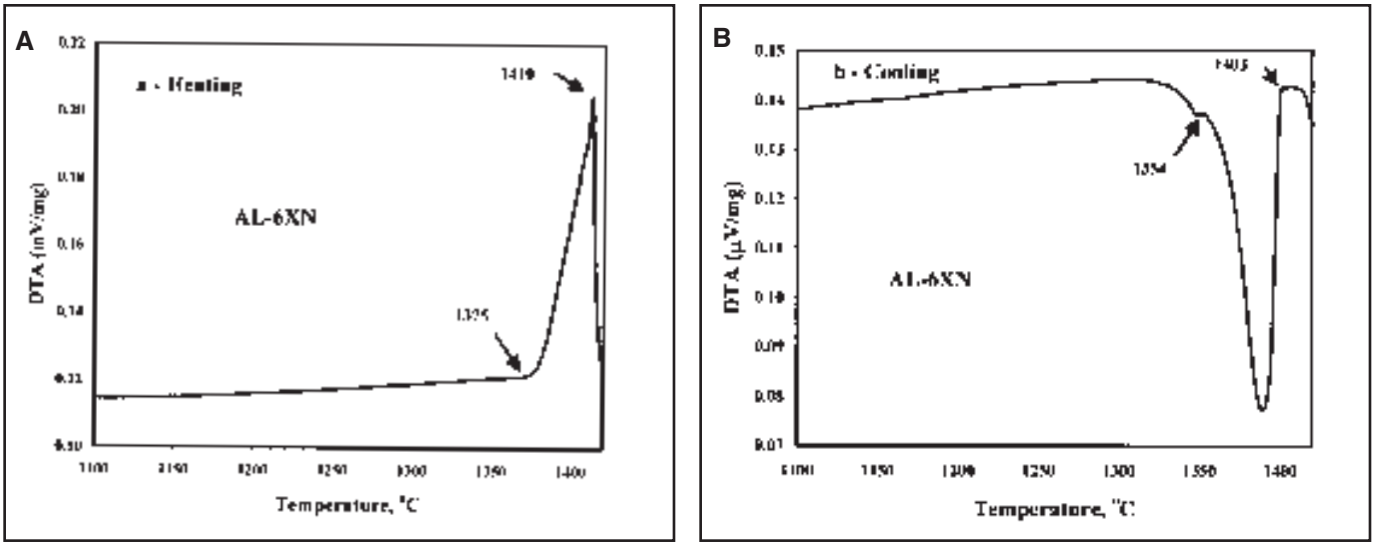

Fig. 13 — DTA traces obtained on AL-6XN base metal. A — During heating; B — during cooling.

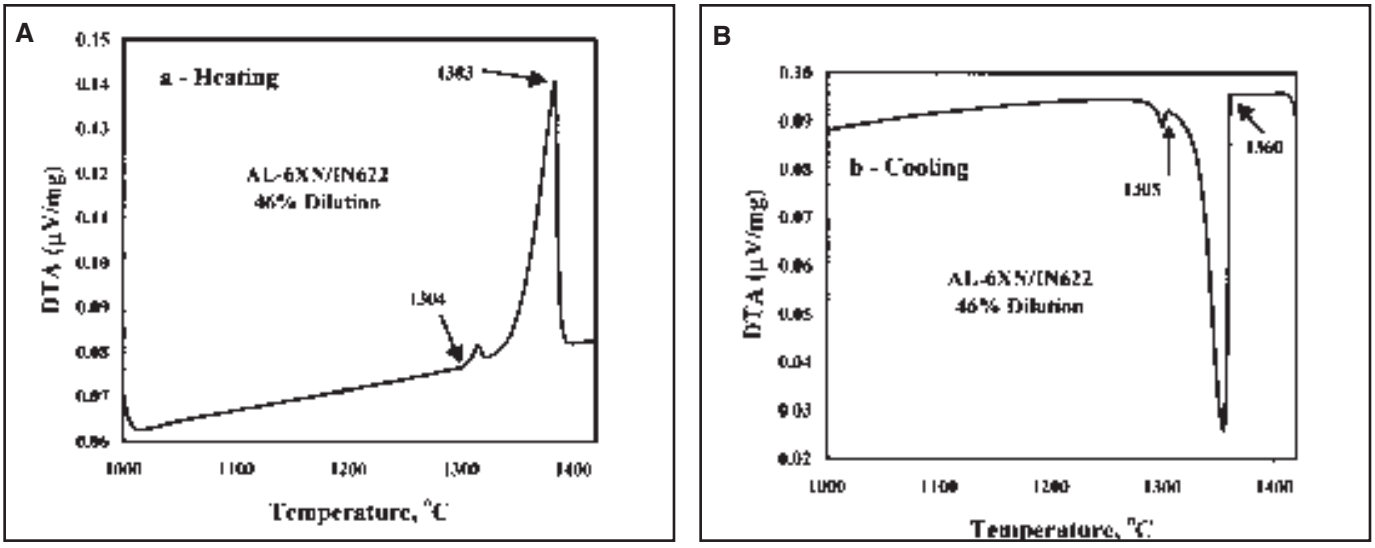

Fig. 14 — DTA traces obtained on weld made with IN622 at 46% dilution. A — During heating; B — during cooling.

primary reaction, in which the γ dendrites reject Mo into the interdendritic liquid. As solidification progresses, the γ dendrites become richer in Mo at the solid/liquid interface until the maximum solid solubility of Mo in austenite is reached at the edge of the γ dendrites. At this point, solidification goes to completion by a $L \rightarrow (\gamma + \sigma)$ reaction, where the σ phase forms in order to dissolve the Mo in the interdendritic liquid. This solidification reaction sequence accounts for the γ dendrites that exhibit a concentration gradient and Mo-rich interdendritic σ phase. The terminal solidification reactions that occur in welds prepared with IN625 are different due to the presence of Nb. It is well established that Nb is a very strong segregant that controls the terminal solidification reactions in Nb-bearing superalloys (Refs. 10–14). Direct evidence to this end is provided in this work by the low k values for Nb reported in Fig. 11. The primary solidification reaction for welds prepared with IN625 is similar and involves the $L \rightarrow \gamma$ reaction. However, both Mo and Nb segregate to the liquid, and solidification goes to completion by two terminal eutectic-type reactions that involve Nb-rich phases: $L \rightarrow (\gamma + NbC)$ followed by ($L \rightarrow \gamma +$ Laves). More details of the segregation behavior and resultant solidification sequences can be found in Ref. 8.

Weldability

It is well known that solidification cracking susceptibility of austenitic alloys depends on the solidification temperature range and amount/distribution of solute rich liquid that exists at the terminal stages of solidification (Refs. 1, 11, 14). A larger solidification temperature range increases the size of the crack-susceptible two-phase solid/liquid zone that trails the liquid weld pool, thus increasing cracking susceptibility. In fact, correlations have been made between the maximum crack length and solidification temperature range (Ref. 11). The amount of terminal solute-rich liquid that forms can be directly assessed by examining the amount of secondary interdendritic phases, since these secondary phases form from the solute-rich liquid. It is generally known (Refs. 11, 13) that solidification cracking susceptibility increases with increasing amount of sec-

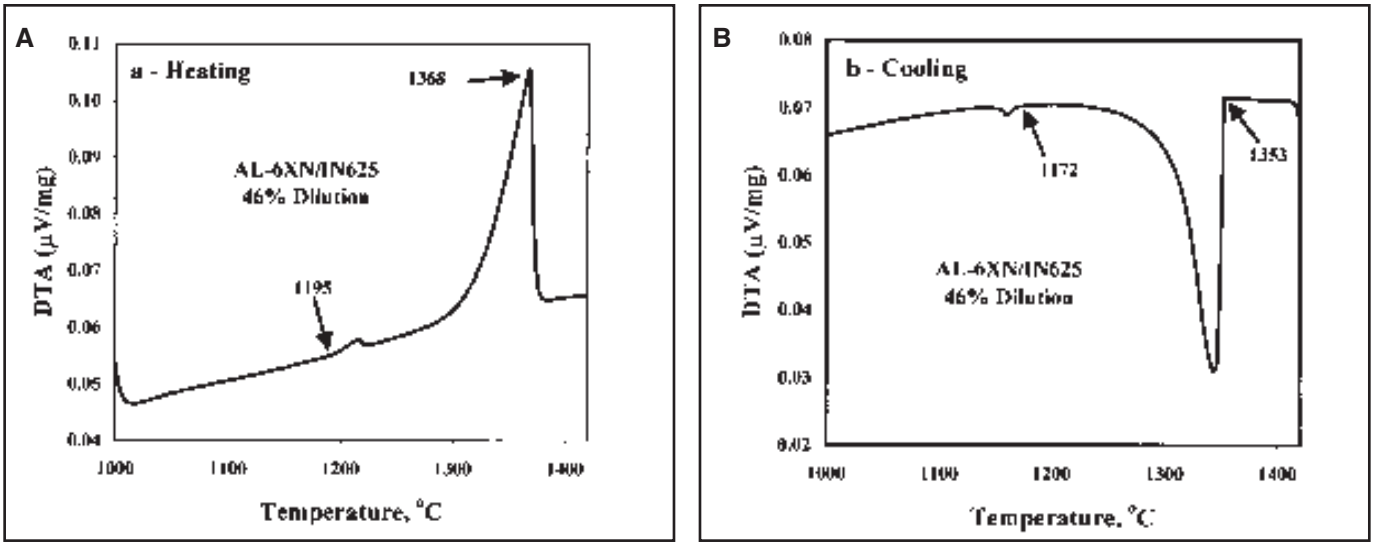

Fig. 15 — DTA traces obtained on weld made with IN625 at 46% dilution. A — During heating; B — during cooling.

ondary constituent up to approximately 10 vol-%, at which point cracking susceptibility begins to decrease with increasing secondary phase amount. The initial increase in cracking susceptibility occurs because the solute-rich liquid wets the grain boundaries and interdendritic regions. Under this condition, shrinkage strains that develop across these partially solidified boundaries cannot be accommodated and cracks form due to boundary separation. With increasing secondary phase amount (above approximately 10 vol-%) the excess solute-rich liquid can lead to back filling of the solidification cracks, thus providing crack healing and reducing cracking susceptibility. The weldability results are provided below and interpreted based on the solidification temperature range (determined from DTA testing) and secondary phase formation.

Figure 12 shows both the maximum and total crack lengths for both sets of samples as a function of dilution level. As previously noted, three samples of each dilution level were tested at an augmented strain of 3.75%, which was determined to be the saturation strain from preliminary experiments. A 316L stainless steel sample, tested under identical conditions, was also added for comparison since this alloy is known to exhibit excellent weldability. The data point for the 316L alloy is located at the 50% dilution level simply for convenience. Average and standard deviation values were determined from at least three samples. The AL-6XN alloy and welds prepared with the nickel-based filler metals were more susceptible to cracking compared to the 316L alloy. This is readily expected because the 316L tested here had a chemical composition that promoted solidification to occur in a primary ferrite mode, which provides excellent cracking resistance. In contrast, the AL-6XN alloy and welds prepared with the nickel-based alloys solidify in a purely austenitic primary mode, and cracking susceptibility is thus relatively higher. Welds prepared with IN625 had the poorest resistance to hot cracking, and the cracking susceptibility increased with decreasing dilution. In contrast, welds prepared with IN622 were more resistant to solidification cracking, and cracking susceptibility is not particularly sensitive to the dilution level.

Table 5 — Summary of Solidification Reaction Temperatures

Alloy/ Weld	Liquidus Temp. (°C)	Terminal Solidification Reaction	Terminal Temp. Reaction (°C)	Solidification Temp. Range (°C)
AL-6XN	1410	$L \rightarrow (\gamma + \sigma)$	1354	54
IN622	1393	$L \rightarrow (\gamma + \sigma)$	1285	108
IN625	1360	$L \rightarrow (\gamma +$ Laves)	1152	208
AL-6XN/IN622 (46% Dilution)	1383	$L \rightarrow (\gamma + \sigma)$	1305	78
AL-6XN/IN625 (46% Dilution)	1368	$L \rightarrow (\gamma +$ Laves)	1172	196

Figures 13 through 15 show DTA traces, which are useful for assessing the influence of filler metal composition on the solidification temperature range. As previously indicated, autogeneous AL-6XN welds and dissimilar welds prepared with IN622 exhibit a two-step solidification reaction sequence represented by $L \rightarrow \gamma$ followed by $L \rightarrow (\gamma + \sigma)$. The welds prepared with IN625 undergo a three-step solidification process: $L \rightarrow \gamma$, $L \rightarrow (\gamma +$ NbC), followed by $L \rightarrow (\gamma +$ Laves). DTA can be used to determine the temperature associated with these reactions and, therefore, can be used to determine the relations between weld composition, solidification temperature range, and resultant weldability. The heating trace shown in Fig. 13A for the AL-6XN base metal exhibits a single endothermic peak that starts at approximately 1375°C. This peak is associated with melting of the austenite matrix. This trace was conducted on the homogeneous, single-phase austenite base metal, which contained no secondary σ phase, and thus no secondary peaks are observed. The apex of the single peak occurs at 1410°C, which represents the liquidus temperature of the alloy. Figure 13B shows the solidification behavior on cooling. Solidification initiates at 1403°C after 7°C of undercooling and terminates at 1354°C by a secondary reaction. The as-solidified microstructure exhibited γ dendrites as the major phase and smaller amounts of interdendritic secondary σ phase. Thus, the large peak initiating at 1403°C is associated with formation of the γ dendrites, and the small secondary peak at 1354°C is associated with the $L \rightarrow (\gamma + \sigma)$ reaction. The solidification temperature range of the weld metal is best represented from DTA data by using the liquidus temperature from the heating trace

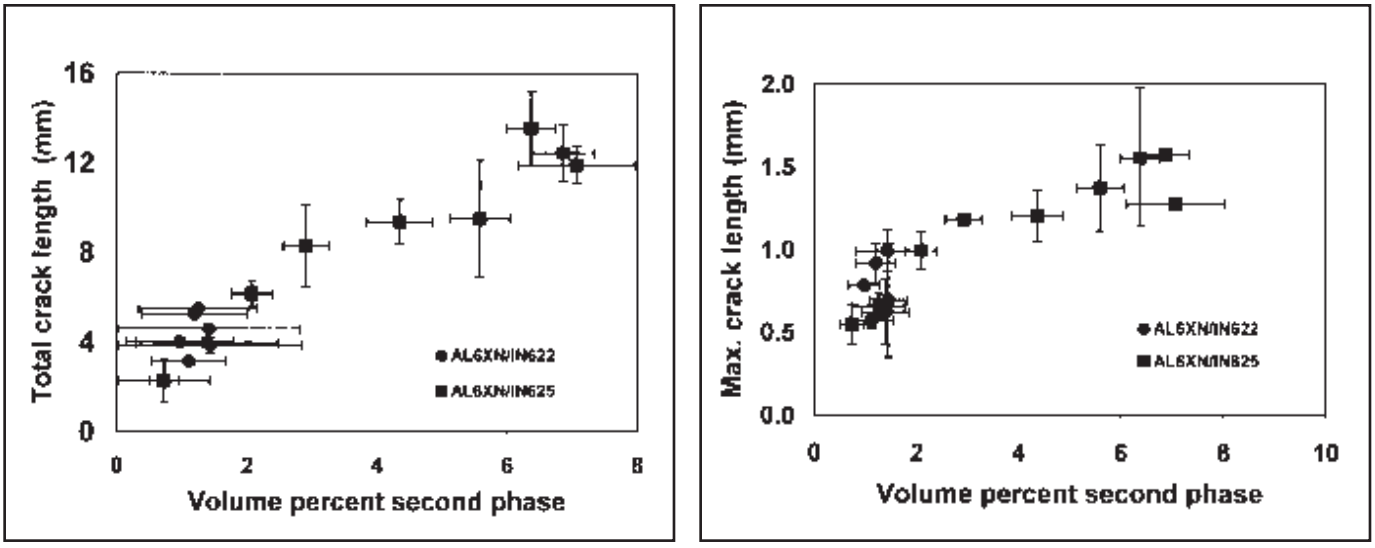

Fig. 16 — Plots. A — Total crack length; B — maximum crack length as a function of the volume-percent second phase.

and the lowest terminal reaction temperature from the cooling trace. The heating trace best represents the liquidus temperature of the weld because solidification in the fusion zone occurs by epitaxial growth off of existing base metal grains and requires no undercooling (Ref. 16). Thus, use of the heating trace avoids the undercooling associated with nucleation in the cooling trace. However, the microsegregation that occurs under the nonequilibrium solidification conditions during cooling of the fusion zone leads to the buildup of solute-rich liquid and formation of secondary phases at low temperature that are best represented by the cooling portion of the DTA trace. Thus, the solidification temperature range of autogeneous welds on AL-6XN is 1410°C – 1354°C = 56°C.

Figures 14 and 15 show the DTA traces of fusion welds prepared with IN622 (Fig. 14) and IN625 (Fig. 15). Each of these welds were prepared at identical dilution levels (46%). Since these traces were conducted on samples extracted from the fusion zone, secondary interdendritic phases are present from the onset of the test, and evidence for liquation of these minor phases is evident in each DTA heating trace. The σ phase liquates at 1304°C in the weld prepared with IN622 — Fig. 14A. The heating trace for the weld prepared with the IN625 displays only one small endothermic peak, but two minor constituents are present in the microstructure (NbC and Laves). Of these two constituents, it is well established that NbC forms at higher temperatures (on the order of 1350°C) and its presence can typically only be detected by DTA techniques in higher carbon alloys, which form relatively large amounts of the NbC constituent (Refs. 11, 12). In contrast, Laves usually forms in higher quantities (and is therefore easier to detect with DTA techniques), and it forms in the temperature range of 1150 to 1200°C. Thus, the minor liquation reaction observed at 1195°C for the weld prepared with IN625 (Fig. 15A) can be linked to the Laves constituent. The liquidus temperatures are 1383 and 1368°C for the welds prepared with IN622 and IN625, respectively. During cooling, the $L \rightarrow (\gamma + \sigma)$ reaction occurs at 1305°C for the weld prepared with IN622, and the solidification temperature range is 78°C. For the weld prepared with the IN625, solidification terminates with the $L \rightarrow (\gamma +$ Laves) reaction at 1172°C, and the solidification temperature range is 196°C. Table 5 summarizes the DTA results. Included in this data are liquidus and terminal reaction temperatures previously reported for IN622 (Ref. 17) and IN625 alloys (Ref. 13.). Thus, the data presented in Table 5 bound the possible range of behavior expected for dissimilar welds on AL-6XN made with IN622 and IN625. This data, along with the quantitative image analysis data shown in Fig. 6, can be used to understand the weldability behavior.

First, the results presented above show that the autogeneous welds on the AL-6XN base metal solidify over a relatively narrow temperature range of 56°C. The IN622 alloy exhibits a similar reaction sequence and solidifies over a larger temperature range of 108°C. The weld between the AL-6XN and IN622 exhibits the same reaction sequence as the "end members," and exhibits an intermediate solidification temperature range of 78°C. This change in solidification temperature range can primarily be attributed to the increase in the $L \rightarrow (\gamma + \sigma)$ reaction temperature, which occurs as the iron content of the weld increases. This influence from iron has also been observed for the $L \rightarrow (\gamma +$ Laves) reaction in welds prepared with IN625 and has been documented in other work as well (Ref. 12). However, the general solidification behavior of fusion welds made with the IN625 is significantly different. In this case, the addition of Nb leads to the formation of Laves at low temperatures and results in a significant widening of the solidification temperature range. This difference in reaction sequence and solidification temperature range accounts, in part, for the observed differences in weldability between the welds prepared with IN622 and IN625.

The data presented in Table 5 does not explain, however, the observed dependence of total and maximum crack length on dilution displayed in Fig. 12. The details of this dependence can be understood by considering the relationship between weld metal dilution and secondary phase formation shown in Fig. 6. As previously discussed, increasing amounts of solute rich liquid (which transforms to secondary phase) lead to increased solidification cracking susceptibility because it interferes with the formation of solid/solid boundaries, thus preventing accommodation of shrinkage strain across the boundaries. Figure 16 shows the direct relation between crack length (both total and maximum) and volume-percent of secondary phase for all the dilution levels. Note that the data for the welds prepared with IN622 are grouped at the lower left portion of the plots where low amounts of secondary phase correspond to low crack lengths (good weldability). It is also interesting to note that, although a wide range of welds were investigated with different compositions, there is a smooth transition

between the data represented by the welds prepared with IN622 and IN625.

In summary, then, the weldability behavior can be interpreted as follows: The solidification cracking resistance of autogeneous AL-6XN welds and welds prepared with IN622 is consistently better than welds prepared with IN625 because the terminal $L \rightarrow (\gamma + \sigma)$ reaction temperature in welds prepared with IN622 is significantly higher than the $L \rightarrow (\gamma +$ Laves) reaction temperature that occurs in welds prepared with IN625. This effectively leads to smaller solidification temperature ranges for autogeneous AL-6XN welds and welds prepared with IN622. The $L \rightarrow (\gamma +$ Laves) reaction is promoted by the Nb additions to IN625. The amount of secondary phase that forms in welds prepared with IN622 is not very sensitive to changes in weld metal composition (dilution) and, thus, solidification cracking resistance is also not a strong function of dilution. (Discussion on the reason for this insensitivity of secondary phase amount on dilution is beyond the scope of the current article and will be the subject of a future article on solidification modeling.) In contrast, the amount of secondary phase that forms in welds made with IN625 depends on the dilution level and, as a result, the weldability also depends on dilution level. In this case, higher dilutions are favored in order to reduce the risk of solidification cracking in the fusion zone. Unfortunately, the higher dilution levels also have reduced nominal and dendrite core Mo concentrations, and are not optimal from a corrosion perspective. Thus, IN622 filler metal is generally favored over IN625 because the weldability is insensitive to dilution.

Conclusions

A study was conducted on microstructural evolution and weldability of dissimilar metal welds between AL-6XN super austenitic stainless steel and two nickel-based alloys, IN625 and IN622. The effect of processing parameters and filler metal chemistry on the final fusion zone composition and microstructure was investigated. These results were related to Varestraint weldability tests. The following conclusions can be drawn from these results:

1) Iron additions to the weld (which occur with increasing dilution) decrease the distribution coefficient of Mo and Nb. This, in turn, produces lower dendrite core concentrations with increasing dilution.

2) Welds prepared with IN622 exhibit a two-step solidification reaction sequence consisting of $L \rightarrow \gamma$ followed by $L \rightarrow (\gamma + \sigma)$. Welds prepared with IN625 exhibit a three step solidification sequence consisting of $L \rightarrow \gamma$, $L \rightarrow (\gamma +$ NbC), and $L \rightarrow (\gamma +$ Laves). The $L \rightarrow (\gamma + \sigma)$ reaction temperature in AL-6XN/IN622 welds depends on dilution level and ranges from 1354°C for "pure" AL-6XN to 1285°C for "pure" IN622. In contrast, the terminal $L \rightarrow (\gamma +$ Laves) reaction temperature in AL-6XN/IN625 welds is considerably lower (approximately 1150°C to 1170°C) and less dependent on weld metal dilution. Thus, welds produced with IN625 have an appreciably wider solidification temperature range.

3) The total amount of secondary phase that forms in welds prepared with IN622 is generally less than about 2 vol-% and does not depend on dilution level. The total amount of secondary phase that forms in welds prepared with IN625 varies from about 7 vol-% at 0% dilution to approximately 2 vol-% at 87% dilution.

4) Welds produced with IN622 exhibit better resistance to solidification cracking than those prepared with IN625. The solidification cracking sensitivity of welds prepared with IN622 is essentially independent of weld metal dilution level, while welds produced with IN625 filler metal exhibit increased cracking susceptibility with decreasing weld metal dilution. The dilution/cracking relation is controlled by the solidification temperature range and amount of secondary phase that forms at the terminal stages of solidification. The good cracking resistance of welds prepared with IN622 is attributed to the small amount of secondary phase and narrow solidification temperature range. The relatively poor cracking resistance of welds prepared with IN625 is attributed to a wide solidification temperature range and increasing amount of secondary phase that forms with decreasing dilution.

Acknowledgments

The authors gratefully acknowledge helpful discussions with Dr. George Yoder from the Office of Naval Research. Financial support for this work was provided by the Office of Naval Research under Contract No. N00014-99-1-0887. Special thanks go to Matthew Perricone of Lehigh for conducting the DTA tests. The AL-6XN material was provided from Allegheny Ludlum by Dr. John Grubb and Ronald Baily and is also appreciated.

References

1. DuPont, J. N. 1999. Microstructural development and solidification cracking susceptibility in the fusion zone of a stabilized stainless steel. *Welding Journal* 78 (7): 253-s to 263-s.

2. Tuthill, A., and Avery, R. 1993. *Welding Journal* 72(2):41-s to 49-s.

3. Gooch, T. G. 1996. *Welding Journal* 75(5): 135-s to 154-s.

4. Baek, K. K., Sung, H. J., Im, C. S., Hong, I. P., and Kim, D. K. 1998. *Proc. Conf. "Corrosion 98."* National Association of Corrosion Engineers, Paper No. 474.

5. Lundin, C. D., Liu, W., Zhou, G., and Qiao, C. Y. 1998. Unmixed zones in arc welds: significance on corrosion resistance of high molybdenum stainless steels. Welding Research Council (WRC), Bulletin No. 428. New York, N.Y.:WRC.

6. Goldstein, J. I., et al. 1992. *Scanning Electron Microscopy and X-ray Microanalysis,* 2nd ed. New York, N.Y.: Plenum Press.

7. Banovic, S. W, DuPont, J. N., and Marder, A. R. 2001. Dilution control in GTA welds involving super austenitic stainless steels and nickel base alloys. *Metallurgical and Materials Transactions B* 1171–1176.

8. Banovic, S. W., DuPont, J. N., and Marder, A. R. 2001. Dilution and microsegregation in dissimilar welds between super austenitic stainless steel and Ni-base alloys. Accepted for publication in *Science & Technology of Welding and Joining*.

9. Grubb, J. F. 1996. *Proc. Conf. "Corrosion 96."* National Association of Corrosion Engineers, Paper No. 426.

10. Cieslak, M. J., Headley, T. J., and Romig, A. D. 1986. *Metallurgical and Materials Transactions A* 17A(11): 2035–2047.

11. DuPont, J. N., Robino, C. V., and Marder, A. R. 1998. Solidification and weldability of Nb-bearing superalloys. *Welding Journal* 77(10): 417-s to 431-s.

12. DuPont, J. N., Robino, C. V., Marder, A. R., Notis, M. R., and Michael, J. R. 1998. Solidification of Nb-bearing superalloys: part I. reaction sequences. *Metallurgical and Material Transactions A* 29A: 2785–2796.

13. Cieslak, M. J. 1991. *Welding Journal* 70(2): 49-s to 56-s.

14. Knorovsky, G. A., Cieslak, M. J., Headley, T. J., Romig, A. D., and Hammetter, W. F. 1989. *Metallurgical Transactions A* 20A: 2149–2158.

15. *ASM Handbook*, Vol. 3, Alloy Phase Diagrams. H. Baker, ed. Materials Park, Ohio: ASM International,

16. David, S. A., and Vitek, J. M. 1989. Correlation between solidification parameters and weld microstructures. *International Materials Review* 34: 213–245.

17. Cieslak, M. J., Headley, T. J., and Romig, A. D. 1986. *Metall Trans A* 17A(11): 2035–2047.